Radical-Radical Reaction Dynamics Probed Using mmW Spectroscopy: Propargyl + NH<sub>2</sub>/ND<sub>2</sub>.

Ranil M. Gurusinghe<sup>1</sup>, Nureshan Dias<sup>1</sup>, Alexander M. Mebel\*<sup>2</sup>, and Arthur G. Suits\*<sup>1</sup>

<sup>1</sup>Department of Chemistry, University of Missouri, Columbia, Missouri 65201, United States

<sup>2</sup>Department of Chemistry and Biochemistry, Florida International University, Miami, Florida 33199, United States

Abstract

We apply chirped-pulse uniform flow millimeterwave (CPUF-mmW) spectroscopy to study the

complex multichannel reaction dynamics in the reaction between the propargyl and amino

radicals (C<sub>3</sub>H<sub>3</sub> + NH<sub>2</sub>/ND<sub>2</sub>), a radical-radical reaction of importance in the gas-phase chemistry of

astrochemical environments and combustion systems. The photolytically-generated radicals are

allowed to react in a well-characterized quasi-uniform supersonic flow, and mmW rotational

spectroscopy (70 - 93 GHz) is used for simultaneous detection of the reaction products: HCN,

HNC, HC<sub>3</sub>N, DCN, DNC, and DC<sub>3</sub>N, while spectral intensities of the measured pure-rotational lines

allow product branching to be quantified. High-level electronic structure calculations were used

for theoretical prediction of the reaction pathways and branching. Experimentally deduced

product branching fractions were compared with the results from statistical simulations based

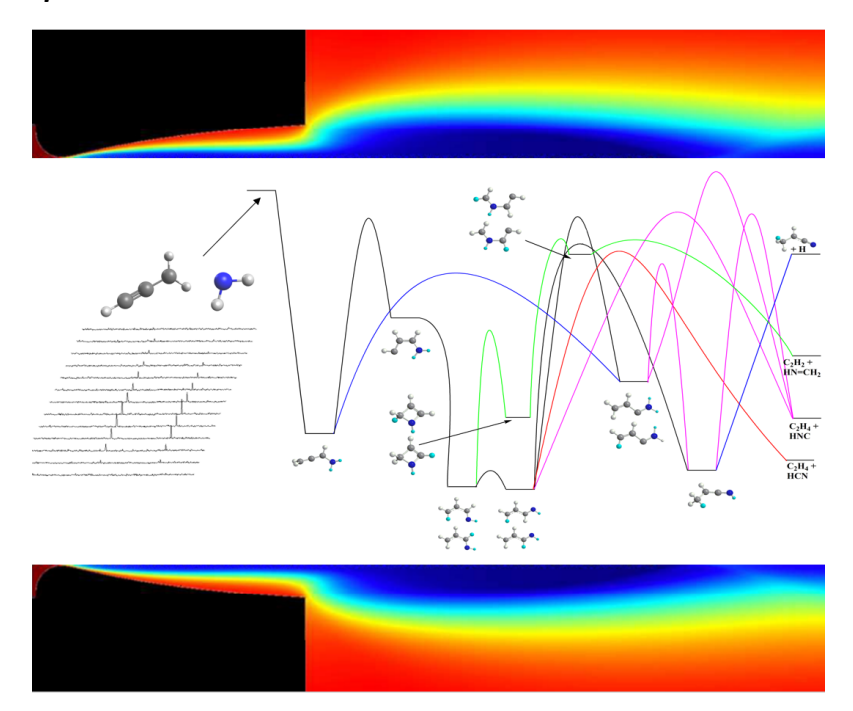
on the RRKM theory. Product branching was found to be strongly dependent on the excess

internal energy of the C<sub>3</sub>H<sub>3</sub> and NH<sub>2</sub>/ND<sub>2</sub> reactants.

E- mail: suitsa@missouri.edu, mebela@fiu.edu

1

## TOC Graphic



Radical-radical reactions are key to understanding the chemistry of environments where reactions of stable species are too slow to proceed and the radical pool is sufficiently concentrated, such as planetary atmospheres or combustion environments. These reactions are barrierless, and kinetic investigations show that the rates of such reactions often increase with decreasing temperature. However, laboratory investigation of the chemical dynamics of radical-radical reactions is challenging. Experimentally, it is difficult to form unstable or highly reactive species at concentrations needed and maintain the reaction medium at desired conditions. Theoretically, it is difficult to model the intermolecular electric multipole interactions and dispersion forces in a radical-radical encounter. Furthermore, for radical-radical systems the reactant energy is generally high on the global potential energy surface, and for polyatomic radical pairs there may be many product channels. Due to these well-known experimental and theoretical challenges, investigations of radical-radical reaction dynamics have been mostly limited to reactions of chemically simpler molecular and atomic radicals.

Despite the challenges, radical-radical reaction kinetics have been successfully studied over the years using mass spectrometric detection, with considerable emphasis placed on hydrocarbon radicals in reaction with themselves or with atoms such as H, N or  $O(^{3}P)$ . The major focus of such studies, conducted at room temperature and above, has been combustion. Crossed-beam methods have also been applied to understand the detailed dynamics of such reactions under single-collision conditions. In 1997, Kaiser *et al.* reported the first such study, of  $C(^{3}P) + C_{3}H_{3}$ , using mass spectrometric detection. Only H-loss giving diacetylene was observed in that reaction. This was followed by many studies of  $O(^{3}P)$  reactions with hydrocarbon radicals, from Choi *et al.* using laser-induced fluorescence (LIF) detection of the OH product and from the

Perugia group using mass spectrometric detection.<sup>7,8</sup> Recent work by Kaiser, Ahmed, and Mebel investigated the role of radical-radical reactions in high-temperature mass growth processes using the reaction between 1-indenyl radical and methyl radical to form naphthalene and other C<sub>10</sub>H<sub>8</sub> isomers. Smith, Sims, and coworkers have used the CRESU technique (French acronym meaning reaction kinetics in uniform supersonic flows) for low-temperature rate determinations of CN + O<sub>2</sub> and CN + NO as prototype "radical-radical" reactions, although in this case one of the reactants is a stable open-shell molecule. 10,11 Rowe and coworkers' CRESU technique uses a Laval nozzle expansion to create a uniform supersonic molecular beam, which acts as a wall-less gasphase flow reactor. 12 The high total molecular density in a uniform flow (1x1016 - 1x1017 molecules/cm<sup>3</sup>) helps to rapidly thermalize the reactants and products through collisions with an inert carrier gas, therefore, very low temperatures (<10 K) can be achieved without any condensation. In two cases, the CRESU technique has been applied to determine the rate coefficient for reactions of two unstable radicals of astrochemical interest, notably by Sims and coworkers for O + OH, and more recently by the Bordeaux group for N + OH. These are challenging experiments in particular owing to the difficulty of determining the radical concentrations needed for absolute rate determination.

All of these experimental studies have employed either laser-induced fluorescence (LIF) or mass spectrometric detection. LIF is well-suited to kinetics measurements in the CRESU environment as the decay of a single reactant may be followed in the uniform flow, but is limited to select atomic species and molecular radicals, notably OH and CN. Mass spectrometry is a universal detection strategy but generally does not give isomer-specific detection and quantitative

branching information is not readily obtained. Following the revolutionary development from Pate and coworkers, rotational spectroscopy has emerged as a powerful alternative strategy for detection and quantitation of transient gas-phase molecules. Rotational spectroscopy provides unambiguous interpretation of a molecule's geometry due to the direct relationship of rotational transition frequencies to the molecule's moments of inertia. It has proven to become a near-universal, reliable detection technique for precise characterization of large peptides, weakly bonded van der Waals complexes, chiral isomers, and reactive open-shell molecules. Here we show it is an ideal detection method for probing complex multichannel radical-radical reactions.

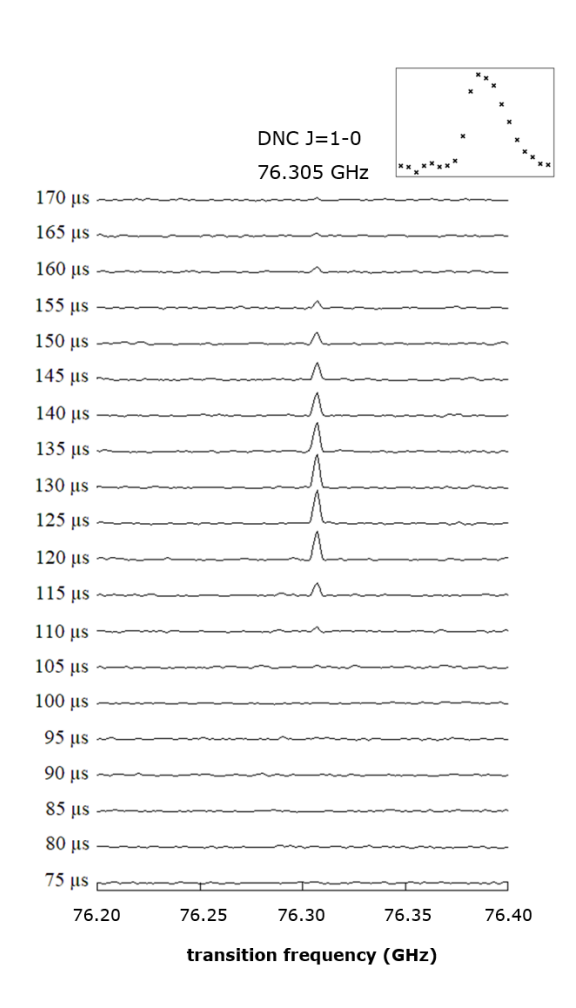
Accurate chemical data, validated by both experiment and theory, are essential to the construction of chemical models that can explain the gas-phase chemistry of the interstellar medium (ISM), planetary atmospheres, and combustion systems. Here we present a detailed investigation of the C<sub>3</sub>H<sub>3</sub> + NH<sub>2</sub>/ND<sub>2</sub> reaction, including multiple product channels and isomerspecific product branching, by combining chirped-pulse mmW spectroscopy in a quasi-uniform flow with high-level molecular orbital and statistical theory calculations. Propargyl has been considered as a possible interstellar molecule and used in models of interstellar chemistry long before its identification in the ISM.<sup>21</sup> The recent discovery of propargyl in the dark cloud TMC-1 and its remarkably high abundance (8.7x10<sup>13</sup> molecules/cm<sup>2</sup> of column density) suggest propargyl may be a key molecule contributing to the chemical complexity in the ISM<sup>22</sup>. Moreover, Miller and Melius showed that recombination of two propargyl radicals is the main route to

produce the first benzene ring in combustion processes, with recent confirmation of this pathway using synchrotron photoionization detection.<sup>23,24</sup> Therefore, propargyl may contribute to molecular weight growth of larger carbonaceous compounds, such as polyaromatic hydrocarbons (PAHs), polycyclic aromatic nitrogen heterocycles (PANHs), and carbonaceous interstellar dust formation, in both highly reactive and non-reactive environments.<sup>25</sup> On the other hand, amino radical has been considered as a central molecule that contributes to the chemical complexity in planetary atmospheres and combustion systems.<sup>26,27</sup> Since ammonia is an important source of atomic hydrogen in the atmospheres of the giant planets, reactions of NH<sub>2</sub> with small unsaturated hydrocarbons have been widely investigated and used in models of the atmospheric chemistry of Jupiter, Saturn, and Titan.<sup>28,29</sup>

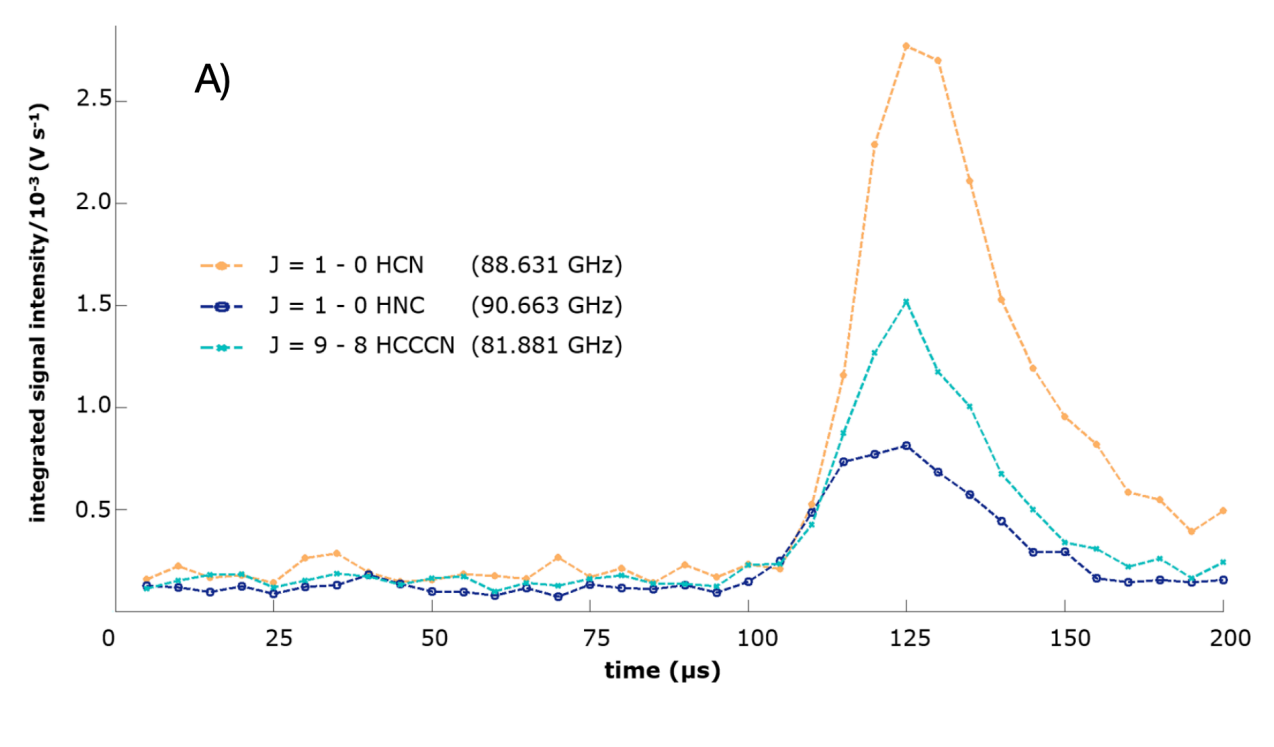
In our chirped-pulse and uniform flow, or CPUF, approach, we combine a CRESU-based pulsed quasi-uniform flow scheme to thermalize radicals in a well-defined low-temperature collisional environment and a chirped-pulse mmW scheme for simultaneous time-dependent detection and quantification of polar gas-phase molecules.<sup>30</sup> Temperature, pressure, and density in the uniform flow are determined by the characteristics of the convergent-divergent Laval nozzle. For optimum sensitivity and resolution in the mmW detection, we have adapted a quasi-uniform flow condition rather than a fully uniform flow.<sup>31</sup> This helium quasi-uniform flow provides a high density region upstream (~10<sup>17</sup> molecules/cm³) that can initiate bimolecular reactions and a low-density region downstream (~10<sup>15</sup> molecules/ cm³) for optimal mmW detection, and it has been well-characterized in previous studies with experimental Pitot measurements and computational fluid dynamics simulations.<sup>31</sup> Propargyl and amino radicals are produced by 193 nm photodissociation (~10 mJ/pulse, 5 x 10<sup>16</sup> photons/cm²) of a gas mixture with 2% propargyl

bromide (C<sub>3</sub>H<sub>3</sub>Br), 2% NH<sub>3</sub> or ND<sub>3</sub>, and helium. Relative product branching of this multichannel reaction was calculated using the integrated signal intensity, transition dipole moment, and partition function associated with each rotational transition and the molecular rotational temperature. The rotational temperature (11 K) was determined in a separate experiment using propionitrile, which has many rotational transitions in our spectral window. In addition, branching results were normalized for mmW power variation at different frequencies. Additional experimental details on our current CPUF setup are given in the S.I.

Reaction products were identified from their vibrational ground state rotational spectra in the 70 - 93 GHz region. Three products: HCN, HNC, and HC<sub>3</sub>N, were identified and quantitated from the C<sub>3</sub>H<sub>3</sub> + NH<sub>2</sub> reaction, while six products: HCN, DCN, HNC, DNC, HC<sub>3</sub>N, and DC<sub>3</sub>N, were identified and quantitated from the C<sub>3</sub>H<sub>3</sub> + ND<sub>2</sub> reaction. Figure 1 shows the typical raw signal, in this case the time evolution of the CPUF-mmW signal of DNC J = 1 - 0 rotational transition. Figure 2a and 2b show the integrated spectral line intensities that were measured at 5 µs time intervals for a total of 170 µs (34 x 5 µs "fast-frames" in the oscilloscope) for all of the products. Given the uniform flow velocity, these time-dependent spectral measurements allow us to determine the locations where the corresponding products were formed within the flow. According to the flow velocity (1600 m s<sup>-1</sup>), nozzle exit to mmW horns distance (8.5 cm), and relative-timing of the laser (6<sup>th</sup> frame = 30  $\mu$ s timepoint), all the products are formed 3 – 10 cm upstream from the nozzle exit. Experimental results in Table 1 and Table 2 show the relative product branching fractions calculated using the integrated signal intensities in frames 22 − 32. In the C<sub>3</sub>H<sub>3</sub> + NH<sub>2</sub> reaction, HCN is the dominant product with a 53% branching and the HCN/HNC ratio is 5.8. The branching fractions are significantly different for the C<sub>3</sub>H<sub>3</sub> + ND<sub>2</sub> reaction, where DNC is the dominant product at 31% and, more interestingly, DNC/DCN ratio is 8.8. In addition, since the molecular partition function strongly depends on the rotational temperature, experimentally determined branching fractions are highly sensitive to the rotational temperature in the probe region. Table S1 of Supporting Information provides an estimate of uncertainties in branching fractions based on a  $11 \pm 3$  K change in rotational temperature.



**Figure 1.** Time evolution of the CPUF-mmW signal of DNC J = 1 - 0 rotational transition in the  $C_3H_3 + ND_2$  reaction. A 193 nm laser pulse, fired at the t = 30  $\mu$ s time point, initiates the reaction via photodissociation of a mixture of  $C_3H_3$ Br,  $ND_3$ , and He.



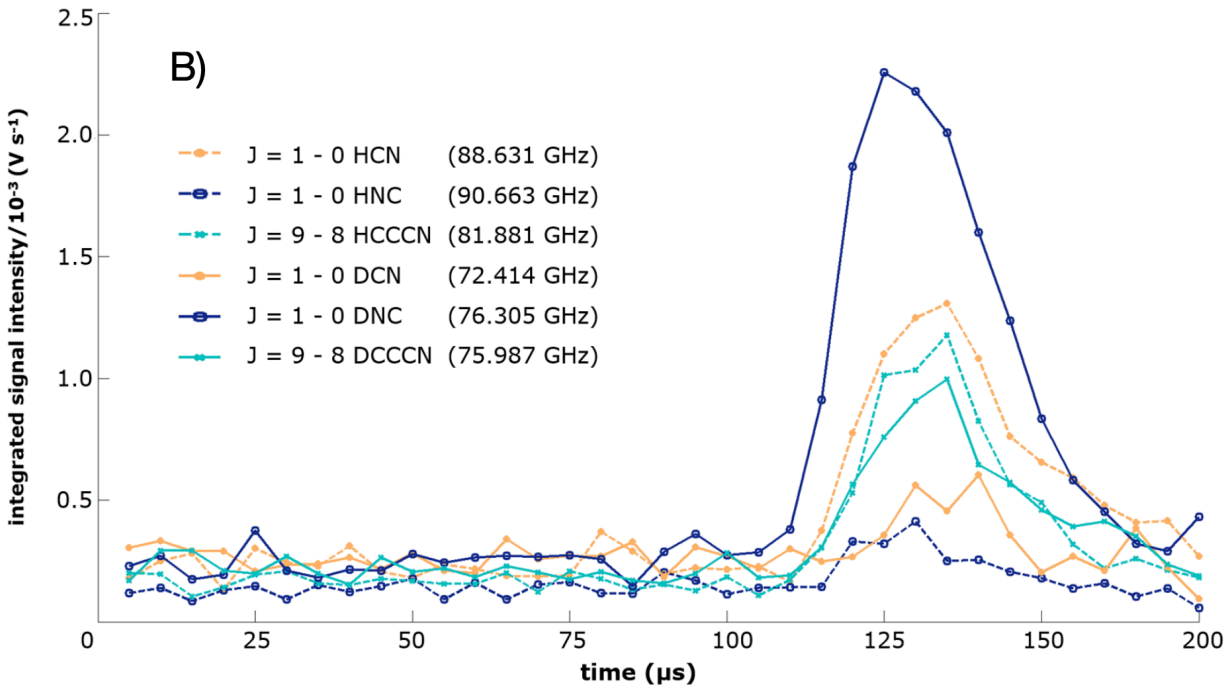


**Figure 2**. A) Time dependence of the HCN, HNC, and HC<sub>3</sub>N rotational signal intensities in the  $C_3H_3 + NH_2$  reaction. B) Time dependence of the HCN, HNC, HC<sub>3</sub>N, DCN, DNC, DC<sub>3</sub>N rotational signal intensities in the  $C_3H_3 + ND_2$  reaction. The broken-lines and solid-lines represent normal and deuterated isotopologues, respectively.

**Table 1.** Experimental and calculated product branching fractions (%) for the  $C_3H_3 + NH_2$  reaction. "nd" is "not detected".

product	experimental branching fractions	calculated branching fractions at different excess energies (kJ/mol)		
		0	100	200
HCN	53	7.0	30	34
HNC	9.1	0.020	2.2	10
NHCH <sub>2</sub>	nd	0.42	3.0	3.9
CH₃CHCN	nd	93	65	50
CH <sub>2</sub> CHCN	nd	0.0	0.080	1.5
HC₃N	38			

**Table 2.** Experimental and calculated product branching fractions (%) for the  $C_3H_3 + ND_2$  reaction. "nd" is "not detected".

product	experimental branching fractions	calculated branching fractions at indicated excess energies (kJ/mol)		
		0	100	200
HCN	19	12	12	11
DCN	3.5	20	17	14
HNC	2.6	0.29	0.70	1.2
DNC	31	28	42	52
NDCDH	nd	1.8	1.8	1.8
$NDCH_2$	nd	3.1	2.6	2.2
CH <sub>2</sub> CHCN	nd	1.9	3.5	5.2
CH <sub>2</sub> DCHCN	nd	33	21	12
$HC_3N$	24			
$DC_3N$	21			

In order to understand the observed product channels and their branching, high-level electronic structure and statistical Rice–Ramsperger–Kassel–Marcus (RRKM) theory calculations were used.<sup>32</sup> Optimized geometries, energetics, and harmonic vibrational frequencies of equilibrium structures and transition states were calculated at the B3LYP/6-311G\*\* level of theory. Connections of the transitions states to corresponding reactants and products were verified using intrinsic reaction coordinate (IRC) analysis.<sup>33</sup> More accurate energies were calculated at the explicitly correlated coupled clusters CCSD(T)-F12/cc-pvqz-f12+ZPE(B3LYP/6-311G\*\*) level of theory and were used to map out the C<sub>3</sub>NH<sub>5</sub> potential energy surface (PES).<sup>34,35</sup> The electronic structure calculations were performed employing the Gaussian 09 and MOLPRO 2010 software

packages.<sup>36,37</sup> A reduced version of this surface focusing on the key features participating in the reaction is shown in Figure 3, while a complete potential energy graph is shown in Figure S1a. In addition, Figure S1b shows H elimination pathways leading to various C<sub>3</sub>NH<sub>4</sub> radicals followed by a second H loss to C<sub>3</sub>NH<sub>3</sub>. Finally, calculated energetics were used in multichannel RRKM calculations using the MESS (Master Equation System Solver) package to determine rate constants of individual reaction steps and product branching fractions at the pressure of 0.1 Torr with He as the bath gas.<sup>38</sup>

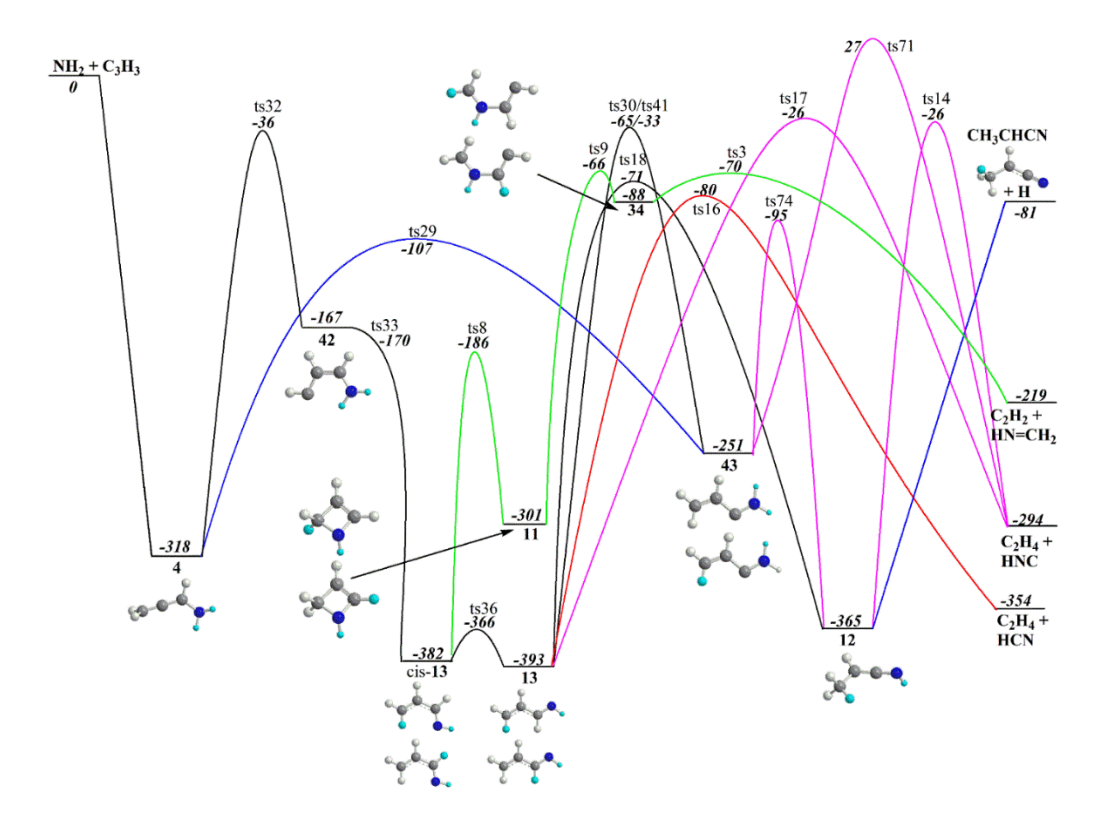


**Figure 3**. Potential energy surface of the  $C_3H_3 + NH_2/ND_2$  reaction showing the major reaction channels, calculated at CCSD(T)-F12/cc-pvqz-f12//B3LYP/6-311G\*\* + ZPE(B3LYP/6-311G\*\*) level of theory. Atoms in blue trace the deuterium atoms in the  $C_3H_3+ND_2$  reaction. Bold italic numbers show relative energies (in kJ/mol) of various species including intermediates, transition states, and products with respect to  $NH_2 + C_3H_3$ .

 $NH_2$  to  $C_3H_3$  addition is fast and barrierless and leads to a deep potential well as the radicals combine to form a stable C–N bond.  $C_3H_3$  in its  $^2B_1$  ground vibronic state, is a resonance stabilized

radical, in which the two resonance forms are the propargyl form (HC=C-CH<sub>2</sub>) and allenyl form (HC=C=CH<sub>2</sub>).<sup>39</sup> The NH<sub>2</sub> addition to the "tail" forms propargylamine, HC=C-CH<sub>2</sub>NH<sub>2</sub>, and to the "head" forms allenylamine, HC(NH<sub>2</sub>)=C=CH<sub>2</sub>, intermediates, which are -299 kJ/mol and -318 kJ/mol below the energy of reactants. As a result of the 193 nm photoexcitation (~6.4 eV), these intermediates may possess significant internal energy to facilitate subsequent isomerization or decomposition pathways. However, the adducts are not expected to re-dissociate into the reactants due to their deep potential well relative to the reactants and the availability of more exoergic decay pathways.

The electronic structure calculations show that all the low-energy reaction pathways leading to the formation of observed products are on the allenylamine PES. The critical hub for these pathways is the 2-propen-1-imine intermediate (CH<sub>2</sub>CHCHNH; *INT13*), from which reaction flux branches into multiple directions. 2-propen-1-imine is formed from allenylamine following subsequent [1,2] and [1,4] H-shifts. In addition, the *cis*- and *trans*-2-propen-1-imine have nearly the same energies (-382 kJ/mol and -393 kJ/mol) and a low barrier (16 kJ/mol) for interconversion.

One facile pathway is predicted for the formation of HCN, which is the direct decomposition of 2-propen-1-imine via ts16 (R1). Ethylene ( $C_2H_4$ ) is a coproduct of this reaction, but the absence of a permanent dipole moment precludes mmW detection.

$$CH2CHCHNH \xrightarrow{ts16 (-80 \text{ kJ/mol})} HCN + C2H4$$
 (R1)

Four decomposition pathways of 2-propen-1-imine are predicted to compete in the formation of HNC. The first one, similar to the HCN formation pathway, is the direct decomposition of 2-propen-1-imine via *ts17* to produce HNC and ethylene (R2).

$$CH_2CHCHNH \xrightarrow{ts17 (-26 \text{ kJ/mol})} HNC + C_2H_4$$
 (R2)

Two other pathways for HNC formation involve the less stable  $CH_2CHCNH_2$  (*INT43*) radical intermediate and the more stable  $CH_3CHCNH$  intermediate (1-propen-1-imine; *INT12*); both are produced from 2-propen-1-imine via H-migrations. Alternatively, HNC can be formed via a secondary decomposition of methanimine (NHCH<sub>2</sub>), for which the [1,1-H<sub>2</sub>] loss from the C atom is the preferable pathway for molecular hydrogen elimination (Figure S1a). For the methanimine pathway, *cis*-2-propen-1-imine undergoes a cyclization to form the four-membered cyclic amine, 2-azetine (*INT11*), followed by a ring-opening through a  $C_{(1)} - C_{(2)}$  bond cleavage to form the radical intermediate  $CH_2NHCHCH$  (*INT34*). Afterward, the decomposition of  $CH_2NHCHCH$  leads to the formation of methanimine and acetylene (R3).

$$CH_2NHCHCH \xrightarrow{ts3 (-70 \text{ kJ/mol})} NHCH_2 + C_2H_2$$
 (R3)

In the secondary decomposition of methanimine,  $H_2$ -loss should prefer the formation of HNC over HCN because [1,1]  $H_2$ -loss from NHCH<sub>2</sub> requires about 42 kJ/mol less energy compared to a [1,1]  $H_2$ -loss from a metastable NCH<sub>3</sub> isomer after a H-shift from the nitrogen to carbon. Moreover, [1,1]  $H_2$ -loss from NH<sub>2</sub>CH isomer has a higher barrier than either of those above.

$$NHCH2 \xrightarrow{[1,1] H-loss} HNC + H2$$
 (R4)

HC<sub>3</sub>N is predicted to be a product of a series of H-losses from the resonantly stabilized radical, CH<sub>3</sub>CHCN. CH<sub>3</sub>CHCN is also formed from 2-propen-1-imine, through the CH<sub>3</sub>CHCNH intermediate (*INT12*). Sequential H-losses from CH<sub>3</sub>CHCN, either by roaming or conventional H-losses, form HC<sub>3</sub>N (R5 and R6). An H<sub>2</sub>-loss from NHCH<sub>2</sub> requires 359 kJ/mol; that is 140 kJ/mol above the energy of the reactants. Considering H<sub>2</sub>-loss from CH<sub>2</sub>CHCN to be similar to a H<sub>2</sub>-loss from ethylene, which requires about 400 kJ/mol, the energy of the corresponding transition state would be also about 140 kJ/mol above the energy of the reactants. For a reaction that occurs at 40 K, these high-barrier H<sub>2</sub>-loss pathways must be slow, and NHCH<sub>2</sub> and CH<sub>2</sub>CHCN (dipole moments,  $\mu_{b,NHCH_2}$  = 1.8 D and  $\mu_{a,CH_2,CHCN}$  = 4.4 D, calculated at MP2/6-311++G\*\*) intermediates should be detectable in the mmW spectrum – unless reactants possess excess internal energy from their preparation.

$$CH_3CHCN \xrightarrow{H-loss} CH_2CHCN + H$$
 (R5)

$$CH_2CHCN \xrightarrow{H_2-loss} HCCCN + H_2$$
 (R6)

We estimated the initial excess internal energy of reactants based on prior reports on photodissociation dynamics of  $C_3H_3Br$  and  $NH_3$ . For 193 nm photodissociation of  $C_3H_3Br$ , Lee*et al.* reported three competing dissociation channels and the translational energy distribution of photoproducts.<sup>40</sup> We estimate an average product internal energy of 338 kJ/mol for  $Br + C_3H_3$  based on the photon energy of 618 kJ/mol (6.4 eV) and C–Br bond dissociation energy of 197 kJ/mol.<sup>41</sup> For 193 nm photodissociation of  $NH_3$ , a well-studied photofragmentation process, Wittig *et al.* showed that  $NH_2$  ( $\widetilde{X}$ ) fragments possess an average internal energy of about 173 kJ/mol (14500 cm<sup>-1</sup>).<sup>42</sup> Therefore,  $C_3H_3$  and  $NH_2/ND_2$  photofragments are formed with high levels

of rotational and vibrational excitation. Following the photolysis, excited radicals are adiabatically cooled during the supersonic expansion. Generally, rotational cooling is held to be much more effective than the vibrational cooling and reactants and products are rapidly rotationally cooled to the translational temperature of the carrier gas (40 K).<sup>43</sup> However, for polyatomic molecules with many internal degrees of freedom and low-frequency vibrational modes, the efficiency of vibrational relaxation can be quite high, particularly in molecule-molecule collisions.<sup>44,45</sup> Furthermore, in the present study reactions occurring in the nozzle throat at room temperature and high pressure also contribute significantly. In any case, given the large initial excitation in these radicals, it is likely that considerable excess internal energy in C<sub>3</sub>H<sub>3</sub> and NH<sub>2</sub>/ND<sub>2</sub> remain as they undergo a fast barrierless addition.

The RRKM rate constants are obtained from microcanonical transition state theory and depend on the total internal energy of the reactants. Thus, given the possibility of significant initial vibrational energy in the reactants, we performed RRKM calculations at the reactants' zero excess internal energy level and at two non-zero excess energy levels, 100, and 200 kJ/mol to obtain energy-specific rate constants and branching. The predicted branching fractions at these three internal energy levels are compared with the experimentally determined branching fractions for the  $C_3H_3 + NH_2$  and  $C_3H_3 + ND_2$  reactions in Table 1 and Table 2, respectively. At the zero excess energy, the RRKM calculations show the  $C_3H_3 + NH_2$  reaction to proceed predominantly by H loss to  $CH_3CHCN$ , with HCN and HNC being minor products. In addition, for the  $C_3H_3 + NH_2$  reaction, zero excess energy calculations highly overestimate the HCN/HNC ratio, 348.5 (theoretically) vs 5.8 (experimentally). For the  $C_3H_3 + ND_2$  reaction, zero excess energy calculations underestimate the DNC/DCN ratio, 1.4 (theoretically) vs 8.8 (experimentally). The

trend we see in experimentally determined product branching is better reproduced when the reactants are assumed to possess 200 kJ/mol excess internal energy. With that excess energy, the calculated HCN/HNC ratio is 3.3. In reaction with the deuterated amino radical (ND<sub>2</sub>), the DNC + C<sub>2</sub>HD pathway is the dominant channel (52%) and the DNC/DCN ratio is 3.6. This suggests highly excited C<sub>3</sub>H<sub>3</sub> and NH<sub>2</sub>/ND<sub>2</sub> radicals may possess excess internal energy of at least  $\sim$ 200 kJ/mol as they react. Thus, we conclude post-photolysis vibrational and rotational relaxation is key to the product distribution and in fact, the overall branching is governed in part by the competition between the reaction and vibrational relaxation. It should also be noted that direct comparison of the product branching ratios computed for the primary C<sub>3</sub>H<sub>3</sub> + NH<sub>2</sub> reaction is not fully warranted if the experimental conditions do not preclude secondary decomposition of the primary products. RRKM calculations for the secondary decomposition channels strongly depend on the internal energy distribution in the primary products which is largely unknown.

Photochemically initiated neutral radical-radical reactions largely contribute to the growth of chemical complexity in the upper atmosphere of giant planets and, especially, of Titan. 46 Titan's atmosphere is particularly of interest due to its similarities to the earth's prebiotic atmosphere. In the upper troposphere and lower stratosphere of Titan, nitrile chemistry and hydrocarbon photolysis by shorter-wavelength light can create a complex reaction network. 47 CPUF-mmW spectroscopy enables investigation of multichannel reaction dynamics by combining a well-defined, wall-less reactor and a near-universal detection scheme. Using the C<sub>3</sub>H<sub>3</sub> + NH<sub>2</sub>/ND<sub>2</sub> reaction, we show that chemical dynamics of a wide variety of reactions can be investigated using the CPUF-mmW approach. Applications of CPUF-mmW extend beyond the investigation of reaction dynamics; future generations of CPUF-mmW experiments will enable precise

measurements of absolute rate coefficients of complex reactions by exploiting its ability to detect and quantify reactants and products simultaneously at well-defined conditions<sup>48</sup>.

## **Supporting Information**

Additional details on the chirped-pulse uniform flow (CPUF) spectroscopy experimental setup and materials used; uncertainties of the experimental product branching fractions; additional details on the potential energy surface and reaction pathways; time-dependent rotational spectra of all detected reaction products; input files used in the MESS (Master Equation System Solver) code.

## Acknowledgments

This work was supported by the NSF under award number CHE-1955239.

## References

- (1) Sims, I. R.; Smith, I. W. M. Rate Constants for the Radical-Radical Reaction Between CN and O<sub>2</sub> at Temperatures down to 99 K. *Chem. Phys. Lett.* **1988**, *151* (6), 481–484.
- (2) Reignier, D.; Stoecklin, T.; Le Picard, S. D.; Canosa, A.; Rowe, B. R. Rate Constant Calculations for Atom–Diatom Reaction Involving an Open-Shell Atom and a Molecule in a  $\Sigma$  Electronic State Application to the Reaction AI( ${}^2P_{1/2,3/2}$ ) +  $O_2(X \, {}^3\Sigma_g^-) \rightarrow AIO(X \, {}^2\Sigma^+) + O({}^3P_{2,1,0})$ . *J. Chem. Soc., Faraday T rans.,* **1998**, *94* (12), 1681–1686.
- (3) Shafir, E. V.; Slagle, I. R.; Knyazev, V. D. Kinetics and Products of the Self-Reaction of Propargyl Radicals. *J. Phys. Chem. A* **2003**, *107* (42), 8893–8903.
- (4) Stief, L. J.; Marston, G.; Nava, D. F.; Payne, W. A.; Nesbitt, F. L. Rate Constant for the Reaction of N(<sup>4</sup>S) with CH<sub>3</sub> at 298 K. *Chem. Phy. Lett.* **1988**, *147* (6), 570–574.
- (5) Vakhtin, A. B.; Murphy, J. E.; Leone, S. R. Low-Temperature Kinetics of Reactions of OH Radical With Ethene, Propene, and 1-Butene. *J. Phys. Chem. A* **2003**, *107* (47), 10055–10062.
- (6) Kaiser, R. I.; Sun, W.; Suits, A. G.; Lee, Y. T. Crossed Beam Reaction of Atomic Carbon,  $C(^3P_j)$ , with the Propargyl Radical,  $C_3H_3(X\ ^2B_2)$ : Observation of Diacetylene,  $C_4H_2(X\ ^1\Sigma_g^+)$ . *J. Chem. Phy.* **1997**, *107* (20), 8713–8716.
- (7) Choi, J.-H. Radical–Radical Reaction Dynamics: A Combined Crossed-Beam and Theoretical Study. *Int. Rev. in Phys. Chem.* **2006**, *25* (4), 613–653.

- (8) Casavecchia, P.; Leonori, F.; Balucani, N. Reaction Dynamics of Oxygen Atoms With Unsaturated Hydrocarbons from Crossed Molecular Beam Studies: Primary Products, Branching Ratios and Role of Intersystem Crossing. *Int. Rev. in Phys. Chem.* **2015**, *34* (2), 161–204.
- (9) Zhao, L.; Kaiser, R. I.; Lu, B.; Xu, B.; Ahmed, M.; Morozov, A. N.; Mebel, A. M.; Howlader, A. H.; Wnuk, S. F. Molecular Mass Growth Through Ring Expansion in Polycyclic Aromatic Hydrocarbons via Radical–Radical Reactions. *Nat. Commun.* **2019**, *10*, 3689.
- (10) Sims, I. R.; Queffelec, J. L.; Defrance, A.; Rebrion-Rowe, C.; Travers, D.; Rowe, B. R.; Smith, I. W. M. Ultra-low Temperature Kinetics of Neutral–Neutral Reactions: The Reaction CN+O<sub>2</sub> Down to 26 K. *J. Chem. Phys.* **1992**, *97* (11), 8798–8800.
- (11) Sims, I. R.; Smith, I. W. M. Gas-Phase Reactions and Energy Transfer at Very Low Temperatures. *Annu. Rev. Phys. Chem.* **1995**, *46* (1), 109–138.
- (12) Potapov, A.; Canosa, A.; Jiménez, E.; Rowe, B. Uniform Supersonic Chemical Reactors: 30 Years of Astrochemical History and Future Challenges. *Angew. Chem. Int. Ed.* **2017**, *56* (30), 8618–8640.
- (13) Daranlot, J.; Jorfi, M.; Xie, C.; Bergeat, A.; Costes, M.; Caubet, P.; Xie, D.; Guo, H.; Honvault, P.; Hickson, K. M. Revealing Atom-Radical Reactivity at Low Temperature Through the N + OH Reaction. *Science* **2011**, *334* (6062), 1538–1541.
- (14) Tizniti, M.; Le Picard, S. D.; Canosa, A.; Sims, I. R.; Smith, I. W. M. Low Temperature Kinetics: The Association of OH Radicals with O<sub>2</sub>. *Phys. Chem. Chem. Phys.* **2010**, *12* (39), 12702-12710.

- (15) Brown, G. G.; Dian, B. C.; Douglass, K. O.; Geyer, S. M.; Shipman, S. T.; Pate, B. H. A Broadband Fourier Transform Microwave Spectrometer Based on Chirped Pulse Excitation. *Rev. Sci. Instrum.* **2008**, *79* (5), 053103.
- (16) León, I.; Alonso, E. R.; Mata, S.; Alonso, J. L. Shape of Testosterone. *J. Phys. Chem. Lett.*2021, 12 (29), 6983–6987.
- (17) Gurusinghe, R. M.; Fox-Loe, A.; Tubergen, M. J. Structures of Guaiacol and the Guaiacol-Argon van Der Waals Complex from Rotational Spectroscopy of Guaiacol Isotopologues. *J. Mol. Struct.* **2021**, *1246*, 131233.
- (18) Patterson, D.; Schnell, M.; Doyle, J. M. Enantiomer-Specific Detection of Chiral Molecules via Microwave Spectroscopy. *Nature* **2013**, *497* (7450), 475–477.
- (19) Pate, B. H.; Evangelisti, L.; Caminati, W.; Xu, Y.; Thomas, J.; Patterson, D.; Perez, C.; Schnell,
  M. Quantitative Chiral Analysis by Molecular Rotational Spectroscopy. *Chiral Analysis*. 2018;
  679–729.
- (20) Evans, C. J.; Needham, L.-M. E.; Walker, N. R.; Köckert, H.; Zaleski, D. P.; Stephens, S. L. The Pure Rotational Spectra of the Open-Shell Diatomic Molecules Pbl and Snl. *J. Chem. Phys.* **2015**, *143* (24), 244309.
- (21) Cherchneff, I. The Formation of Polycyclic Aromatic Hydrocarbons in Evolved Circumstellar Environments. *EAS Publ. Ser.* **2011**, *46*, 177–189.
- (22) Agúndez, M.; Cabezas, C.; Tercero, B.; Marcelino, N.; Gallego, J. D.; de Vicente, P.; Cernicharo, J. Discovery of the Propargyl Radical (CH<sub>2</sub>CCH) in TMC-1: One of the Most Abundant

Radicals Ever Found and a Key Species for Cyclization to Benzene in Cold Dark Clouds. *A&A* **2021**, *647*, L10.

- (23) Miller, J. A.; Melius, C. F. Kinetic and Thermodynamic Issues in the Formation of Aromatic Compounds in Flames of Aliphatic Fuels. *Combust. Flame* **1992**, *91* (1), 21–39.
- (24) Zhao, L.; Lu, W.; Ahmed, M.; Zagidullin, M. V.; Azyazov, V. N.; Morozov, A. N.; Mebel, A. M.; Kaiser, R. I. Gas-Phase Synthesis of Benzene via the Propargyl Radical Self-Reaction. *Sci. Adv.* **2021**, *7* (21) 1-9.
- (25) Tielens, A. G. G. M. The Molecular Universe. Rev. Mod. Phys. 2013, 85 (3), 1021–1081.
- (26) van Dishoeck, E. F.; Jansen, D. J.; Schilke, P.; Phillips, T. G. Detection of the Interstellar NH<sub>2</sub> Radical. *ApJ* **1993**, *416*, L83-86.
- (27) Glarborg, P.; Miller, J. A.; Ruscic, B.; Klippenstein, S. J. Modeling Nitrogen Chemistry in Combustion. *Prog. Energy Combust. Sci.* **2018**, *67*, 31–68.
- (28) Moses, J. I.; Visscher, C.; Keane, T. C.; Sperier, A. On the Abundance of Non-Cometary HCN on Jupiter. *Faraday Discuss.* **2010**, *147*, 103-136.
- (29) Strobel, D. F. Photochemistry of the Reducing Atmospheres of Jupiter, Saturn and Titan. *Int. Rev. Phys. Chem.* **1983**, *3* (2), 145–176.
- (30) Abeysekera, C.; Zack, L. N.; Park, G. B.; Joalland, B.; Oldham, J. M.; Prozument, K.; Ariyasingha, N. M.; Sims, I. R.; Field, R. W.; Suits, A. G. A Chirped-Pulse Fourier-Transform Microwave/Pulsed Uniform Flow Spectrometer. II. Performance and Applications for Reaction Dynamics. *J. Chem. Phys.* **2014**, *141* (21), 214203.

- (31) Broderick, B. M.; Suas-David, N.; Dias, N.; Suits, A. G. Isomer-Specific Detection in the UV Photodissociation of the Propargyl Radical by Chirped-Pulse mm-Wave Spectroscopy in a Pulsed Quasi-Uniform Flow. *Phys. Chem. Chem. Phys.* **2018**, *20* (8), 5517–5529.
- (32) Marcus, R. A. Unimolecular Dissociations and Free Radical Recombination Reactions. *The J. Chem. Phys.* **1952**, *20* (3), 359–364.
- (33) Fukui, K. The Path of Chemical Reactions The IRC Approach. *Acc. Chem. Res.* **1981**, *14* (12), 363–368.
- (34) Adler, T. B.; Knizia, G.; Werner, H.-J. A Simple and Efficient CCSD(T)-F12 Approximation. *J. Chem. Phys.* **2007**, *127* (22), 221106.
- (35) Knizia, G.; Adler, T. B.; Werner, H.-J. Simplified CCSD(T)-F12 Methods: Theory and Benchmarks. *J. Chem. Phys.* **2009**, *130* (5), 054104.
- (36) Frisch, M. J.; Trucks, G. W.; Schlegel, H. B.; Scuseria, G. E.; Robb, M. A.; Cheeseman, J. R.; Scalmani, G.; Barone, V.; Mennucci, B.; Petersson, G. A.; Nakatsuji, H.; Caricato, M.; Li, X.; Hratchian, H. P.; Izmaylov, A. F.; Bloino, J.; Zheng, G.; Sonnenberg, J. L.; Hada, M.; Ehara, M.; Toyota, K.; Fukuda, R.; Hasegawa, J.; Ishida, M.; Nakajima, T.; Honda, Y.; Kitao, O.; Nakai, H.; Vreven, T.; Montgomery, J. A.; Peralta, J. E.; Ogliaro, F.; Bearpark, M.; Heyd, J. J.; Brothers, E.; Kudin, K. N.; Staroverov, V. N.; Kobayashi, R.; Normand, J.; Raghavachari, K.; Rendell, A.; Burant, J. C.; Iyengar, S. S.; Tomasi, J.; Cossi, M.; Rega, N.; Millam, J. M.; Klene, M.; Knox, J. E.; Cross, J. B.; Bakken, V.; Adamo, C.; Jaramillo, J.; Gomperts, R.; Stratmann, R. E.; Yazyev, O.; Austin, A. J.; Cammi, R.; Pomelli, C.; Ochterski, J. W.; Martin, R. L.; Morokuma, K.; Zakrzewski, V. G.; Voth, G.

- A.; Salvador, P.; Dannenberg, J. J.; Dapprich, S.; Daniels, A. D.; Farkas, Ö.; Foresman, J. B.; Ortiz, J. V.; Cioslowski, J.; Fox, D. J. Gaussian 09 Revision A.1; **2009**.
- (37) Werner, H.-J.; Knowles, P. J.; Lindh, R.; Manby, F. R.; Schütz, M.; Celani, P.; Korona, T.; Rauhut, G.; Amos, R. D.; Bernhardsson, A. MOLPRO, Version 2010.1, A Package of Ab Initio Programs; University of Cardiff: Cardiff: U.K., **2010**.
- (38) Georgievskii, Y.; Miller, J. A.; Burke, M. P.; Klippenstein, S. J. Reformulation and Solution of the Master Equation for Multiple-Well Chemical Reactions. *J. Phys. Chem. A* **2013**, *117* (46), 12146–12154.
- (39) Tanaka, K.; Sumiyoshi, Y.; Ohshima, Y.; Endo, Y.; Kawaguchi, K. Pulsed Discharge Nozzle Fourier Transform Microwave Spectroscopy of the Propargyl Radical (H₂CCCH). *J. Chem. Phys.* **1997**, *107* (8), 2728–2733.
- (40) Lee, Y.-R.; Lin, S.-M. Photodissociation of CH≡CCH<sub>2</sub>X (X=Br and Cl) by Translational Spectroscopy. *J. Chem. Phys.* **1998**, *108* (1), 134–141.
- (41) Szwarc, M.; Ghosh, B. N.; Sehon, A. H. The C–Br Bond Dissociation Energy in Benzyl Bromide and Allyl Bromide. *J. Chem. Phys.* **1950**, *18* (9), 1142–1149.
- (42) Koplitz, B.; Xu, Z.; Wittig, C. Product Energy Distributions from the 193 nm Photodissociation of NH<sub>3</sub>. *Chem. Phys. Lett.* **1987**, *137* (6), 505–509.
- (43) Levy, D. H. The Spectroscopy of Very Cold Gases. *Science* **1981**, *214* (4518), 263–269.

- (44) Chang, C.-H.; Nesbitt, D. J. Spectroscopy and Dynamics of Jet-Cooled Polyynes in a Slit Supersonic Discharge: Sub-Doppler Infrared Studies of Diacetylene HCCCCH. *J. Phys. Chem. A* **2015**, *119* (28), 7940–7950.
- (45) Dias, N.; Joalland, B.; Ariyasingha, N. M.; Suits, A. G.; Broderick, B. M. Direct versus Indirect Photodissociation of Isoxazole from Product Branching: A Chirped-Pulse Fourier Transform mm-Wave Spectroscopy/Pulsed Uniform Flow Investigation. *J. Phys. Chem. A* **2018**, *122* (38), 7523–7531.
- (46) Blitz, M. A.; Seakins, P. W. Laboratory Studies of Photochemistry and Gas Phase Radical Reaction Kinetics Relevant to Planetary Atmospheres. *Chem. Soc. Rev.* **2012**, *41* (19), 6318-6347.
- (47) Wilson, E. H.; Atreya, S. K. Chemical Sources of Haze Formation in Titan's Atmosphere. *Planet. Space Sci.* **2003**, *51* (14–15), 1017–1033.
- (48) Gurusinghe, R. M.; Dias, N.; Krueger, R.; Suits, A. G. Uniform Supersonic Flow Sampling for Detection by Chirped-Pulse Rotational Spectroscopy. *J. Chem. Phys.* **2021**, (in press).